American Journal of Engineering Research (AJER)
e-ISSN : 2320-0847 p-ISSN : 2320-0936
Volume-02, Issue-08, pp-90-107
www.ajer.org

Research Paper Open Access

Investigation of Brazed Plate Heat Exchangers With Variable Chevron Angles

S. Muthuraman
Professor, Higher College of Technology, Oman

Abstract: - Experiments to measure the condensation heat transfer coefficient and the pressure drop in brazed plate heat exchangers (BPHEs) were performed with the refrigerants R410A and R22. Brazed plate heat exchangers with different chevron angles of 45°, 35°, and 20° were used. Varying the mass flux, the condensation temperature, and the vapor quality of the refrigerant, we measured the condensation heat transfer coefficient and the pressure drops. Both the heat transfer coefficient and the pressure drop increased proportionally with the mass flux and the vapor quality and inversely with the condensation temperature and the chevron angle.

Keywords*: Compact heat exchanger, narrow channel, corrugation, CFD, Nusselt number, pressure drop, condensation, brazed plate heat exchanger, R410a, chevron angle, correlation.*

I. INTRODUCTION

Plate heat exchangers (PHEs) were introduced in the 1930s and were almost exclusively used as liquid/liquid heat exchangers in the food industries because of their ease of cleaning. Over the years, the development of the PHE has generally continued towards larger capacity, as well as higher working temperature and pressure. Recently, a gasket sealing was replaced by a brazed material, and each thermal plate was formed with a series of corrugations (herringbone or chevron). These greatly increased the pressure and the temperature capabilities.

The corrugated pattern on the thermal plate induces a highly turbulent fluid flow. The high turbulence in the PHE leads to an enhanced heat transfer, to a low fouling rate, and to a reduced heat transfer area. Therefore, PHEs can be used as alternatives to shell-and-tube heat exchangers. Due to ozone depletion, the refrigerant R22 is being replaced by R410A (a binary mixture of R32 and R125, mass fraction 50 %/50 %). R410A approximates an azeotropic behavior since it can be regarded as a pure substance because of the negligible temperature gliding. The heat transfer and the pressure drop characteristics in PHEs are related to the hydraulic diameter, the increased heat transfer area, the number of the flow channels, and the profile of the corrugation waviness, such as the inclination angle, the corrugation amplitude, and the corrugation wavelength. These geometric factors influence the separation, the boundary layer, and the vortex or swirl flow generation. However, earlier experimental and numerical works were restricted to a single-phase flow. Since the advent of a Brazed PHE (BPHE) in the 1990s, studies of the condensation and/or evaporation heat transfer have focused on their applications in refrigerating and air conditioning systems, but only a few studies have been done. Much work is needed to understand the features of the two-phase flow in the BPHEs with alternative refrigerants. Xiaoyang *et al.*, [1] experimented with the two-phase flow distribution in stacked PHEs at both vertical upward and downward flow orientations. They indicated that non-uniform distributions were found and that the flow distribution was strongly affected by the total inlet flow rate, the vapor quality, the flow channel orientation, and the geometry of the inlet port Holger [2].Theoretically predicted the performance of chevron-type PHEs under single-phase conditions and recommended the correlations for the friction factors and heat transfer coefficients as functions of the corrugation chevron angles. Lee *et al.*, [3] investigated the characteristics of the evaporation heat transfer and pressure drop in BPHEs with R404A and R407C. Kedzierski [4] reported the effect of inclination on the performance of a BPHE using R22 in both the condenser and the evaporator. Several single-phase correlations for heat transfer coefficients and friction factors have been proposed, but few correlations for the two-phase flow have been proposed. Yan *et al.*, [5] suggested a correlation of condensation with a chevron

angle of 30 for R134a. Yan *et al*., reported that the mass flux, the vapor quality, and the condensation pressure affected the heat transfer coefficients and the pressure drops. Hieh and Lin [6] developed the correlations for evaporation with a chevron angle of 30 for R410A.

The main objective of this work was to experimentally investigate the heat transfer coefficients and the pressure drops during condensation of R410A inside BPHEs. Three BPHEs with different chevron angles of 45, 35, and 20 were used. The results were then compared to those of R22. The geometric effects of the plate on the heat transfer and the pressure drop were investigated by varying the mass flux, the quality, and the condensation temperature. From the results, the geometric effects, especially the chevron angle, must be considered to develop the correlations for the Nusselt number and the friction factor. Correlations for the Nusselt number and the friction factor with the geometric parameters are suggested in this study.

Experiments to measure the condensation heat transfer coefficient and the pressure drop in brazed plate heat exchangers (BPHEs) were performed with the refrigerants R410A and R22. Brazed plate heat exchangers with different chevron angles of 45°, 35°, and 20° were used. Varying the mass flux, the condensation temperature, and the vapor quality of the refrigerant, we measured the condensation heat transfer coefficient and the pressure drops. Both the heat transfer coefficient and the pressure drop increased proportionally with the mass flux and the vapor quality and inversely with the condensation temperature and the chevron angle.

Correlations of the Nusselt number and the friction factor with the geometric parameters are suggested for the tested BPHEs. In an effort to study and optimize the design of a plate heat exchanger comprising of corrugated walls with herringbone design, a CFD code is employed. Due to the difficulties induced by the geometry and flow complexity, an approach through a simplified model was followed as a first step. This simple model, comprised of only one corrugated plate and a flat plate, was constructed and simulated. The Reynolds numbers examined are 400, 900, 1000, 1150, 1250 and 1400. The SST turbulence model was preferred over other flow models for the simulation.

The case where hot water (60^oC) is in contact with a constant-temperature wall (20^oC) was also simulated and the heat transfer rate was calculated. The results for the simplified model, presented in terms of velocity, shear stress and heat transfer coefficients, strongly encourage the simulation of one channel of the typical plate heat exchanger, i.e. the one that comprises of two corrugated plates with herringbone design having their crests nearly in contact. Preliminary results of this latter work, currently in progress, comply with visual observations.

In recent years, compact heat exchangers with corrugated plates are being rapidly adopted by food and chemical process industries, replacing conventional shell-and-tube exchangers. Compact heat exchangers consist of plates embossed with some form of corrugated surface pattern, usually the chevron (herringbone) geometry[1].The plates are assembled being abutting, with their corrugations forming narrow passages. This type of equipment offers high thermal effectiveness and close temperature approach, while allowing ease of inspection and cleaning [1],[2]. In order to be able to evaluate its performance, methods to predict the heat transfer coefficient and pressure drop must be developed. In this direction, CFD is considered an efficient tool for momentum and heat transfer rate estimation in this type of heat exchangers.

The type of flow in such narrow passages, which is associated with the choice of the most appropriate flow model for CFD simulation, is still an open issue in the literature. Due to the relatively high pressure drop, compared to shell-and-tube heat exchangers for equivalent flow rates, the Reynolds numbers used in this type of equipment must be lower so as the resulting pressure drops would be generally acceptable[1]. Moreover, when this equipment is used as a reflux condenser, the limit imposed by the onset of flooding reduces the maximum Reynolds number to a value less than 2000[3]. Ciofalo et al.[4], in a comprehensive review article concerning modeling heat transfer in narrow flow passages, state that, for the Reynolds number range of 1,500-3,000, transitional flow is expected, a kind of flow among the most difficult to simulate by conventional turbulence models.

On the other hand, Shah & Wanniarachchi[1] declare that, for the Reynolds number range 100-1500, there is evidence that the flow is already turbulent, a statement that is also supported by Vlasogiannis et al.[5], whose experiments in a plate heat exchanger verify that the flow is turbulent for Re>650. Lioumbas et al.[6], who studied experimentally the flow in narrow passages during counter-current gas-liquid flow, suggest that the flow exhibits the basic features of turbulent flow even for the relatively low gas Reynolds numbers tested (500<Re<1200).Focke & Knibbe[7] performed flow visualization experiments in narrow passages with corrugated walls. They concluded that the flow patterns in such geometries are complex, due to the existence of secondary swirling motions along the furrows of their test section and suggest that the local flow structure controls the heat transfer process in such narrow passages.

The most common two-equation turbulence model, based on the equations for the turbulence energy k and its dissipation ε, is the k-ε model[8]. To calculate the boundary layer, either "wall functions" are used, overriding the calculation of k and ε in the wall adjacent nodes[8], or integration is performed to the surface,

using a "low turbulent Reynolds (*low-Re*) *k-ε*" model[9]. Menter & Esch[9] state that, in standard *k-ε* the wall shear stress and heat flux are over predicted (especially for the lower range of the Reynolds number encountered in this kind of equipment) due to the over prediction of the turbulent length scale in the flow reattachment region, which is a characteristic phenomenon occurring on the corrugated surfaces in these geometries. Moreover, the standard *k-ε*, model requires a course grid near the wall, based on the value of y^+=11 [9],[10], which is difficult to accomplish in confined geometries. The low-Re *k-ε* model, which uses "dumping functions" near the wall[8],[9], is not considered capable of predicting the flow parameters in the complex geometry of a corrugated narrow channel[4], requires finer mesh near the wall, is computationally expensive compared to the standard *k-ε* model and it is unstable in convergence.

An alternative to *k-ε* model, is the *k-ω* model, developed by Wilcox[11]. This model, which uses the turbulence frequency *ω* instead of the turbulence diffusivity *ε*, appears to be more robust, even for complex applications, and does not require very fine grid near the wall[8]. However, it seems to be sensitive to the free stream values of turbulence frequency *ω* outside the boundary layer. A combination of the two models, *k-ε* and *k-ω*, is the *SST* (Shear-Stress Transport) model, which, by employing specific "blending functions", activates the Wilcox model near the wall and the *k-ε* model for the rest of the flow[9] and thus it benefits from the advantages of both models. Some efforts have been made wards the effective simulation of a plate heat exchanger. Due to the modular nature of a compact heat exchanger, a common practice is to think of it as composed of a large number of unit *cells* (Representative Element Units, *RES*) and obtain results by using a single cell as the computational domain and imposing periodicity conditions across its boundaries[4],[12]. However, the validity of this assumption is considered another open issue in the literature [4].

II. EXPERIMENTAL FACILITY

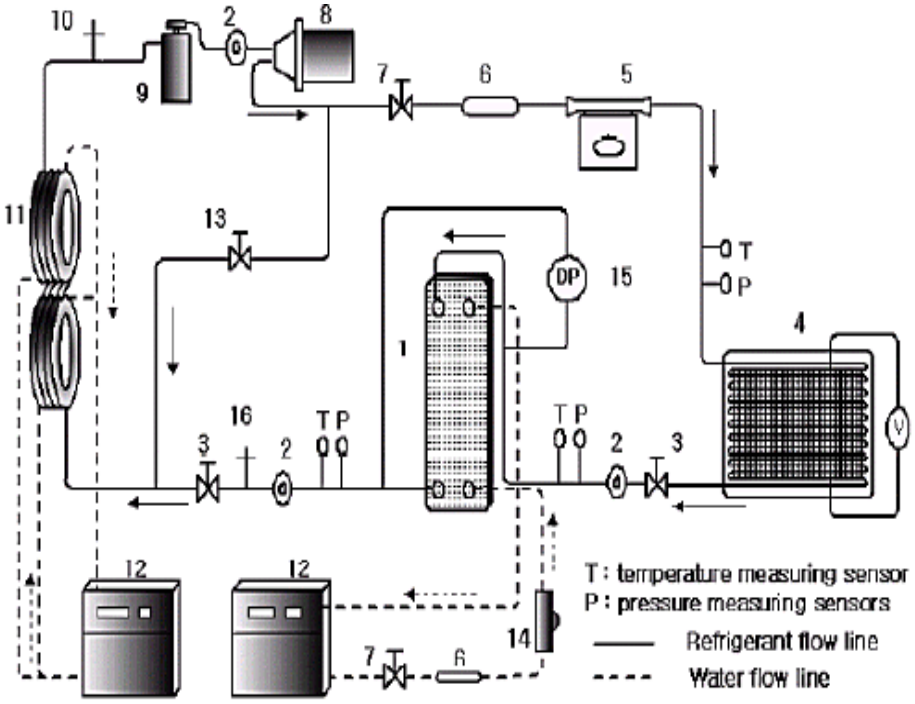

1. Plate heat exchanger	9. Liquid receiver
2. Sight glass	10. Charging port
3. On-off valve	11. Double-pipe heat exchanger
4. Pre-heater	12. Chiller
5. Mass flow meter	13. By-pass valve
6. Filter & dryer	14. Volumetric flow meter
7. Check valve	15. Differential pressure transducer
8. Magnetic gear pump	16. Discharge port

Fig. 1. Schematic diagram of the experimental system.

The experimental facility is capable of determining in plate heat transfer coefficients and measuring the pressure drops for the refrigerants. It consists of four main parts: a test section, a refrigerant loop, two water loops, and a data-acquisition system. A schematic of the test facility used in this study is shown in Figure-1, and detailed descriptions of the four main parts are mentioned below.

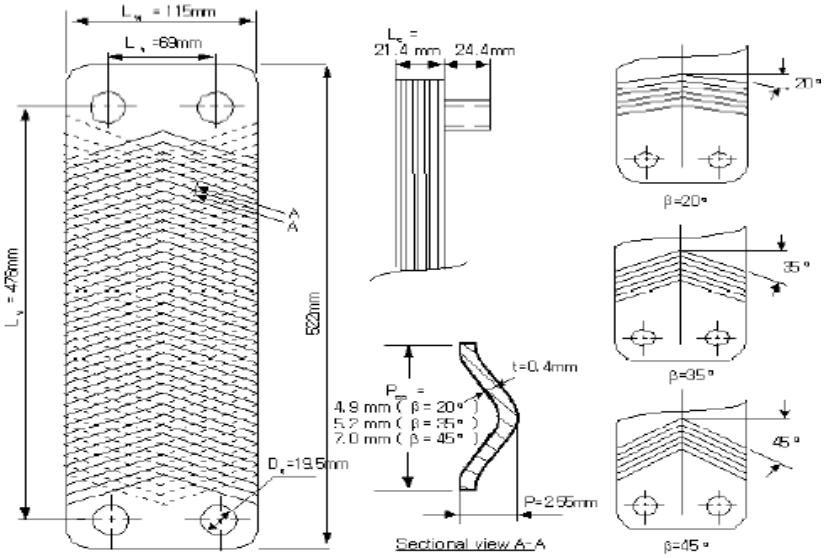

Fig. 2. Dimensions of the brazed plate heat exchangers.

1.1 Brazed plate heat exchangers

Three BPHEs with chevron angles of 45°, 35°, and 20° were used as the test sections. The angles of corrugation were measured from the horizontal axis. Each BPHE was composed of 4 thermal plates and 2 end plates, forming 5 flow channels. The dimensions of the BPHEs are shown in Figure-2. The refrigerant and cooling water were directed into the alternate passages between the plates through corner ports, creating counter flow conditions. The cooling water owed from the bottom to the top of every other channel on the basis of a central channel. On the other hand, the refrigerant owed from the top to the bottom in the rest of them.

1.2 Refrigerant loop

Refrigerant was supplied to the test section at specific conditions (i.e., temperature, flow rate, and quality) through the refrigerant loop. This loop contained a pre-heater, a double-pipe heat exchanger, a receiver, a magnetic gear pump, a differential pressure transducer, and a mass flow meter. Also included were thermocouples probes and pressure taps at the inlet/outlet of the test section. The refrigerant pump was driven by a DC motor which was controlled by a variable DC output motor controller.

The refrigerant flow rate was measured by using a mass flow meter installed between the magnetic gear pump and the pre-heater with an accuracy of _0.5 %. The pre-heater located before the test section was used to evaporate the refrigerant to a specified vapor quality at the inlet of the test section. The pressure drop of the refrigerant owing through the test section was measured with the differential pressure transducer, to an accuracy of _0.25 kPa. The refrigerant through the test section was subcooled at a double-pipe heat exchanger by the water cooled by the chiller and went into a liquid receiver. The subcooled refrigerant returned to the magnetic gear pump and circulated through the refrigerant loop repeatedly. Calibrated T-type thermocouples were used to measure the temperatures of the refrigerant at the inlet/outlet of the test section. The entire loop was insulated with fiberglass to prevent heat transfer to the environment.

1.3 Water loop

There are two closed water loops in this facility. One is for determining the condensation heat flux at the test section. The other is for making the subcooled refrigerant state at two double-pipe heat exchangers before it enters the magnetic gear pump. The water flow rates of the test section were measured by using a turbine flow meter, and T-type thermocouples were installed to evaluate the gain of the heat flux of the water of the test section.

1.4 Data acquisition

The data were recorded by a computer-controlled data-acquisition system with 40 channels scanned at the speed of 30 data per minute. The temperature and the pressure of both fluids were continuously recorded, and the thermodynamic properties of the refrigerant were obtained from a computer program. After steady-state conditions had been reached in the system, all measurements were taken for 10 minutes.

III. DATA REDUCTION AND UNCERTAINTY ANALYSIS

The hydraulic diameter of the channel, D_h, is defined as

D_h= 4XChannel flow area/Wetted perimeter=$4bL_w/2L_w\emptyset$ (1)

Where is φ=1.17. This value is given by the manufacturer.

The mean channel spacing, b, is defined as

b = p - t; t= Plate Thickness (2)

and the plate pitch p can be determined as, N_t=Total Number of plates

$$p= L_c/N_t-1 \quad (3)$$

The procedures to calculate the condensation heat transfer coefficient of the refrigerant side are described below. At first, the refrigerant quality at the inlet of the test section (x_{in}) should be selected to evaluate the condensation heat at a given quality. Its value is calculated from the amount of heat given by a pre-heater, which is the summation of the sensible heat and the latent heat:

$Q_{pre}= Q_{sens}+ Q_{lat}$

$$= m_rC_{p,r}(T_{r,sat}-T_{r,pre,in}) + m_ri_{fg}x_{in} \quad (4)$$

The refrigerant quality at the inlet of the test section can be written as

$$X_{in} = 1/i_{fg} [Q_{pre}/m_r –C_{p,r} (T_{r, sat} – T_{r,pre,in})] \quad (5)$$

The power gained by the pre-heater is calculated by measuring the voltage and the current with a power meter. The change in the refrigerant quality inside the test section was evaluated from the heat transferred in the test section and the refrigerant mass flow rate (6)

$$\Delta x=x_{in}-x_{out}=Q_w/m_rXi_{fg} \quad (6)$$

The condensing heat in the test section was calculated from an energy balance with water:

$$Q_w=m_wC_{p,w}(T_{w,out}-T_{w,in}) \quad (7)$$

The heat transfer coefficient of the refrigerant side (hr) was evaluated from the following equation:

$$1/h_r= (1/U)-(1/h_{w)}-R_{wall} \quad (8)$$

The overall heat transfer coefficient was determined using the log mean temperature difference

$$U=Q_w/A \text{ X } LMTD$$

$$LMTD=(T_{r,out}-T_{w,in})-(T_{r,in}-T_{w,out})/\ln\{(T_{r,out}-T_{w,in})-(T_{r,in}-T_{w,out})\} \quad (9)$$

The heat transfer coefficient of the water side (h_w) was obtained by using Eq. (10). Equation (10) was developed from the single-phase water to water pre-tests by K_{im} [7]. If the least-squares method and the multiple regression method are used, the heat transfer coefficient of the water side is correlated in terms of the Reynolds number, the Prandtl number, and the chevron angle:

$$h_w=0.295(k_w/D_{Eq})Re^{0.64}Pr^{0.32}(\pi/2-\beta)^{0.09} \quad (10)$$

The thermal resistance of the wall is negligible compared to the effect of convection. For the vertical downward flow, the total pressure drop in the test section is defined as

$$\Delta P_{total}=\Delta P_{fr}+\Delta P_a+\Delta P_s+\Delta P_p \quad (11)$$

And ΔP_{total} is measured by using a differential pressure transducer. The two-phase friction factor, f, is defined as

$$\Delta P_{fr}=fL_vN_{cp}G^2_{Eq}/D_h\rho_f \quad (12)$$

The port pressure loss in this experiment was less than 1 % of the total pressure loss. The static head loss can be written as and it has a negative value for vertical downward flow. The acceleration pressure drop for condensation is expressed as

$$\Delta P_p=1.4G^2{}_p/(2\rho_m) \quad (13)$$

An uncertainty analysis was done for all the measured data and the calculated quantities based on the methods described by Moffat [9]. The detailed results of the uncertainty analysis are shown in Table-1.

Table 1. Estimated uncertainty

Parameters	Uncertainty
Temperature	±0.2 ^{0}C
Pressure	±4.7 Pa
Pressure Drop	±250 Pa
Water Flow Rate	±2%
Refrigerant mass flux	±0.5%
Heat flux of test section	±5.7%
Vapor Quality	±0.03
Heat Transfer coefficients of water side	±10.1%
Heat transfer coefficients of refrigerant	±9.1%

Where

$$G_p=4m_{Eq}/\pi D^2_p \quad (14)$$

And

$$(1/\rho_m) = (x/\rho_g) + [(1-x)/\rho_f]. \quad (15)$$

The equivalent mass flow rate, m_{eq}, is defined as

$$m_{eq} = m\,[1-x+x(\rho_f/\rho_g)^{0.5} \quad (16)$$

The port pressure loss in this experiment was less than 1% of the total pressure loss. The static head loss can be written as

$$\Delta P_s = \rho_m g L_v \quad (17)$$

And it has a negative value for vertical downward flow, The acceleration pressure drop for condensation is expressed as

$$\Delta P_a = -\,[(G^2_{eq}x/\rho_{fg})in - (G^2_{eq}x/\rho_{fg})_{out}] \quad (18)$$

IV. RESULTS AND DISCUSSIONS

The condensation heat transfer coefficients and the pressure drops of R410A and R22 were measured in three BPHEs with chevron angles of 20°, 35°, and 45° by varying the mass flux (13 - 34 kg/m^{2}s), the vapor quality (0.9 - 0.15), and the condensing temperature (20°C and 30°C) under a given heat flux condition (4.7 -5.3 kW/m^2). R22 was tested under identical experimental conditions for comparison with R410A.

4.1 Flow regime

Before the behaviors of heat transfer are considered, it is necessary to predict what flow regime exists at a given set of operating conditions. The detailed flow regime map for the PHE has not been proposed yet because of the difficulty of flow visualization. Vlasogiannis *et al*., [10] suggested the criterion of a two-phase flow regime for a PHE in terms of superficial liquid (jf) and vapor velocities (jg) by using water and air under adiabatic conditions. They only simulated a mixture of water and air as a two-phase fluid. According to their work, the flow patterns in a PHE are significantly different from those inside the vertical round tubes. They

detected 3 types of flow patterns. The first was a gas continuous pattern with a liquid pocket at flow water flow rates (jf < 0.025 m/s) over wide range of air flow rates.

The second was the slug flow pattern, which was detected at sufficiently high air (jg > 2 m/s) and water flow rates (jf > 0.025 m/s). Thirdly, the liquid continuous pattern with a gas pocket or a gas bubble at the high water flow rates (jf >0.1 m/s) and low air flow rates (jg < 1 m/s).According to the flow regime map proposed by Vlasogiannis *et al*., the expected flow pattern in this experimental study is the gas continuous flow pattern with liquid pockets. However, their flow regime map has a significant limitation for use since many important features, such as the phase-change, the heating or cooling conditions, the densities or specific volumes of the working fluids, the geometries of the PHEs, etc., were not considered in detail. According to the flow regime map proposed by Crawford *et al*. [11], which was developed for vertical downward flow in a round tube, all experimental flow patterns are located in the intermittent flow regime, but this flow regime can not represent the correct flow regime in a BPHE due to the different geometries.

4.2 Condensation heat transfer

Figure-3 shows the effects of the refrigerant mass flux, the chevron angle, and the condensation temperature on the averaged heat transfer coefficient for R410A. The term "averaged heat transfer coefficient" means the average of the heat transfer coefficients calculated by varying the quality of the refrigerant from 0.15 to 0.9, and the coefficients were obtained from Eq. (19):

$$H_{averged} = \Sigma h_{loca} l x_{local\ /\ } x_{local} \qquad (19)$$

Where h_l is the local heat transfer coefficient at the local vapor quality. The experimental results indicate that the averaged heat transfer coefficients vary proportionally with the mass flux and inversely with the chevron angles and the condensation temperature. The small chevron angle forms narrow pitches to the flow direction, creating more abrupt changes in the velocity and the flow direction, thus increasing the effective contact length and time in a BHPE. The zigzag flow increases the heat transfer, and the turbulence created by the shape of the plate pattern is also important in addition to the turbulence created by the high flow rates. Increasing the mass flux at a given condensation temperature showed that the differences in the averaged heat transfer coefficients were significantly enlarged with decreasing chevron angle. This indicates that a PHE with the small chevron angle is more effective at a large mass flux (Gc > 25 kg/m^{2}s) than at a small mass flux.

The averaged heat transfer coefficient of R410A decreases with increasing condensation temperature. The vapor velocity is a more influential factor than the liquid film thickness for the heat transfer. Vapor bubbles in the flow enhance the disturbance in the bubble wake as a turbulence promoter, and the turbulence induced by the vapor bubbles increases with the vapor velocity. Also, since the specific volume of the vapor increases with decreasing condensation temperature, the vapor velocity increases for a fixed mass flux and quality. The vapor velocity at 20°C is faster than that at 30°C. The rates of the averaged heat transfer coefficients between condensation temperatures of 20°C and 30°C increased 5 % for a chevron angle of 45°, 9 % for 35°, and 16 % for 20°. These results show that different chevron angles lead partly to different flow pattern. Thus, we may conclude that the flow regime map should be modified by geometric considerations. The heat transfer coefficients in the high-quality region (fast velocity region) are larger than those in the low-quality region (slow velocity region). As mentioned above, this happens because the vapor velocity is the dominant effect on the heat transfer mechanism.

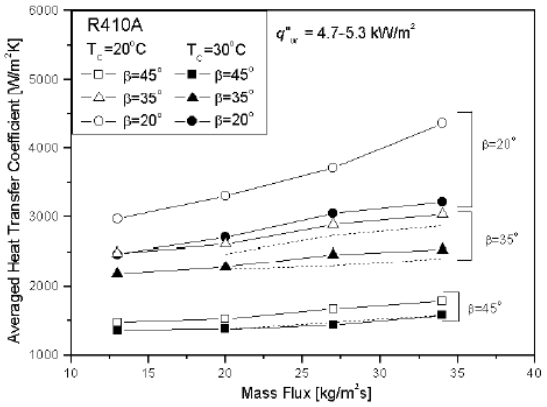

Fig. 3. Effect of mass flux on the averaged condensation heat transfer coefficient.

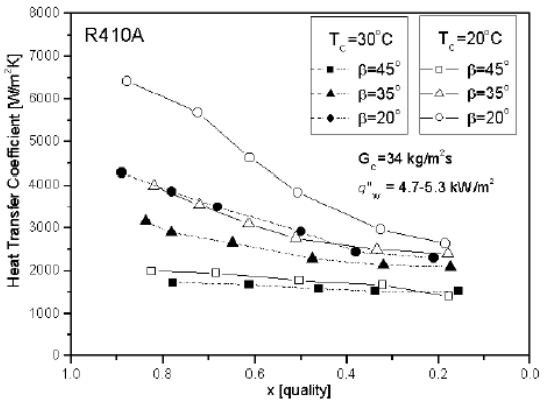

Fig. 4. Effect of quality on the condensation heat transfer coefficient.

Increasing the vapor quality at the same mass flux induces a faster bubble velocity, which increases the turbulence level and the convection heat transfer coefficient. The difference of heat transfer coefficients between the low-quality region and the high-quality region becomes larger with decreasing chevron angle. The PHE with a low chevron angle shows a better heat transfer performance in the high-quality region (i.e., the high vapor velocity region). Figure-4 also shows the variation of the heat transfer coefficients with the condensation temperatures. Like Figure-3, the heat transfer coefficients decreased with increasing condensation temperature. Also, the variations of the heat transfer coefficients with the condensation temperature are larger in the high-quality region. From the experimental results in Figures, 3 and 4, lowering the chevron angle and the condensation temperature gives the desired heat transfer effect.

4.3 Frictional pressure loss

The frictional pressure loss in a BPHE is obtained by subtracting the acceleration pressure loss, the static head loss, and the port pressure loss from the total pressure loss. Figure-5 shows the trend of the pressure drop along the mass flux, and Figure-6 shows the trend of the pressure drop along the quality at a mass flux of 34 kg/m^{2}s and a heat flux of 4.7-5.3 kW/m^2. The frictional pressure drops in the BPHEs increase with increasing mass flux and quality and decreasing condensation temperature and chevron angle. This trend is similar to that of the condensation heat transfer. As mentioned above, since the vapor velocity is much faster than the liquid velocity during the two-phase flow in the tube, the vapor velocity is the dominant influence on the pressure drop, as well as the heat transfer. A high vapor velocity also tends to increase the turbulence of the flow. From Figures 3, 4, 5 and 6, we may concluded that since the trends of the the condensation heat transfer and the pressure loss in BPHEs are similar, those effects must be carefully considered in the design of a BPHE.

4.4 Comparison of R410A with R22

The ratios of R410A to R22 for the condensation heat transfer coefficients and pressure drops at a condensation temperature of 30°C are shown in the Figure-7. The ratios for the heat transfer coefficients are relatively constant in the range of 1 -1.1, regardless of the mass flux, while the ratios for the pressure drops decrease with increasing mass flux, except for the data at a chevron angle of 20° in the present experimental range. For a chevron angle of 20°, the heat transfer ratios of R410A to R22 are about 1.1, and the pressure drop ratios about 0.8, which is a 10 % higher heat transfer and a 20 % lower pressure drop.The smaller specific volume of the vapor of R410A relative to that of R22 makes the vapor velocity slower and yields a small pressure drop under the same conditions of the mass flux. While the two fluids have almost equal values of their latent heats, the liquid-phase thermal conductivity of R410A is larger than that of R22. The higher thermal conductivity for R410A helps to produce better heat transfer even if a reduction in the specific volume occurs. Also, a BPHE with a small chevron angle is known to have more effective performance from the ratios when replacing R22 with R410A.

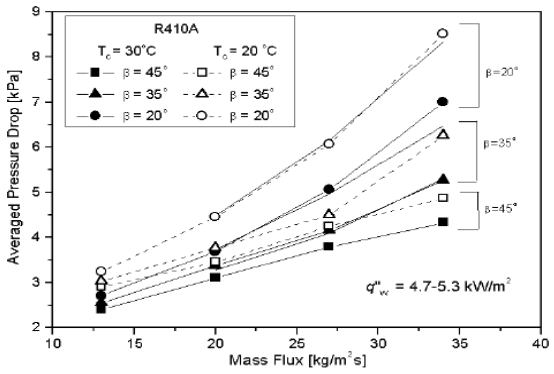

Fig. 5. Variation of the averaged condensation pressure drop with mass flux.

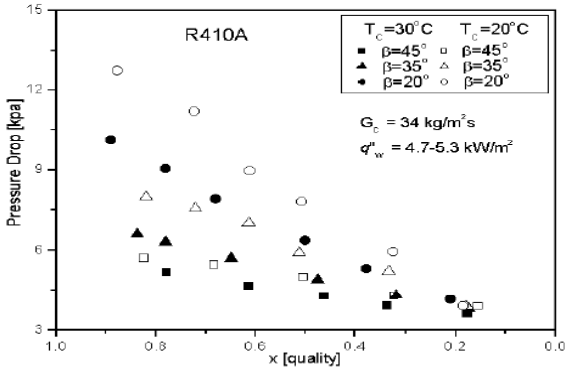

Fig. 6. Variation of the condensation pressure drop with quality.

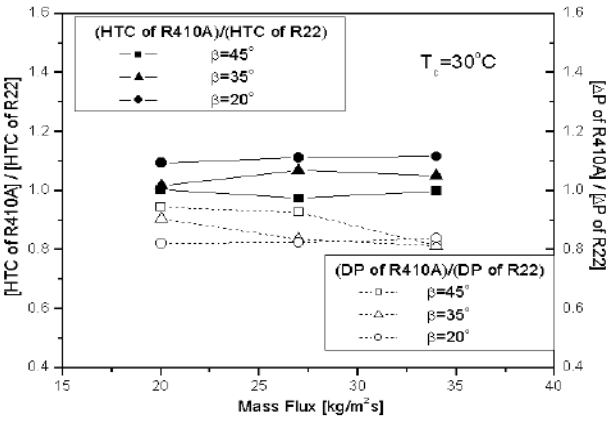

Fig. 7. Condensation heat transfer coefficient ratio and pressure drop ratio between R410A and R22.

4.5 Correlations of Nusselt number and friction factor for tested BPHEs

Based on the experimental data, the following correlations for Nu and f during condensation for the tested BPHEs are established: Where G_{e1}, G_{e2}, G_{e3}, and G_{e4} are non-dimensional geometric parameters that involve the corrugation pitch, the equivalent diameter, and the chevron angle. Re_{Eq} is the equivalent Reynolds number, and G_{Eq} the equivalent mass flux: where G_c is the channel mass flux. The suggested correlations for the Nusselt number and the friction factor can be applied in the range of Re_{Eq} from 300 to 4000. Figure-8(a) shows a comparison of the Nusselt number among the experimental data, the correlation proposed in this paper, and the correlation of Yan *et al.*, [5]. The correlation of Yan *et al.*, is

$$N_u = G_{e1} Re_{Eq}^{Ge1} Pr^{1/3} \quad (20)$$

$$Ge_1 = 11.22\,(p_{co}/D_h)^{-2.83}\,(\Pi/2 - \beta)^{-4.5} \quad (21)$$

$$Ge_2 = 0.35\,(p_{co}/D_h)^{0.23}\,(\Pi/2 - \beta)^{1.48} \quad (22)$$

$$f = Ge_3 Re_{Eq}^{Ge4} \quad (23)$$

$$Ge_3 = 3521.1\,(p_{co}/D_h)^{4.17}\,(\Pi/2 - \beta)^{-7.75} \quad (24)$$

$$Ge_4 = -1.024\,(p_{co}/D_h)^{0.0925}\,(\Pi/2 - \beta)^{-1.3} \quad (25)$$

$$Re_{Eq} = G_{Eq} D_h / \mu_f \quad (26)$$

$$G_{Eq} = G_c[1-x+x(\rho_f/\rho_g)^{1/2} \quad (27)$$

$$G_c = m / N_{ep} b L_w \quad (28)$$

and is obtained from one PHE with a chevron angle of 30° for R134a. Regardless of the BPHE types and refrigerants, most of the experimental data are within 20 % for the correlation proposed in this paper.

The correlation of Yan *et al.*(5), matched the data relatively well for β: 20 and 35 within30 %, but over-predicted the data quite a bit for 45. This discrepancy results from the correlation of Yan *et al.*, being developed for only a +30 PHE. Also,the correlation of Yan *et al.*

$$Nu = 4.118 Re_{eq}^{0.4} Pr^{1/3} \quad (29)$$

for the Nusselt number only adopted the equivalent Reynolds number and Prandtl number without any geometric parameters. Because a BPHE has a strong geometric effect, the correlation with geometric parameters must be developed for general applications. The root-mean-square (r.m.s.) of the deviations is defined as

$$\text{r.m.s.} = \sqrt{1/N_{data}\,\Sigma(Nu_{pred} - Nu_{exp}/Nu_{exp})^2 \times 100}(\%) \quad (28)$$

The r.m.s. deviation for the correlation of Yan *et al.*, [Eq. (29)] is 50.2 % and for Eq. (20), it is only 10.9 %. Figure-8(b) shows a comparison of the friction factor between the experimental data and the proposed

correlation. Similar to the correlation of the Nusselt number, the correlation of the friction factor includes the equivalent Reynolds number and the geometric parameters. Regardless of the BPHE types and refrigerants, most of the experimental data are within 15 % of the correlation proposed in this paper; the r.m.s. deviation for Eq. (23) is 10 %.

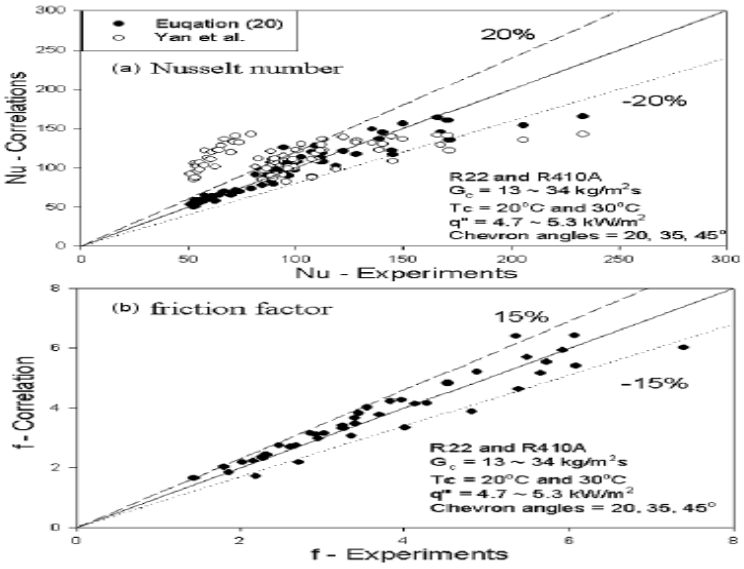

Fig. 8. Comparison of the correlations with the experimental data.

V. 5. STUDY OF A SIMPLIFIED GEOMETRY

In an effort to simulate the flow configuration, a ***simple*** channel was designed and constructed in order to conduct experiments and obtain formation on the flow pattern prevailing inside the furrows of the conduit. The flow configuration, apart from affecting the local momentum and heat transfer rates of a plate heat exchanger, suggests the appropriate flow model for the CFD simulation. A module of a plate heat exchanger is a single pass of the exchanger, consisting of only two plates. The simple channel examined is a single pass made of Plexiglas (***Figure 9***). It is formed by only ***one*** corrugated plate comprised of fourteen equal sized and uniformly spaced corrugations as well as a flat plate and it is used for pressure drop measurements and flow visualization. Details of the plate geometry are presented in ***Table 2***. This model was chosen in an attempt to simplify the complexity of the original plate heat exchanger and to reduce the computational demands. The geometry studied in the CFD simulations (similar to the test section) is shown in ***Figure 10***. The Reynolds numbers examined are 400, 900, 1000, 1150, 1250 and 1400, which are based on the distance between the plates at the entrance (d=10mm), the mean flow velocity and the properties of water at 60°C. In addition to isothermal flow, heat transfer simulations are carried out for the same Reynolds numbers, where hot water (60°C) is cooled in contact with a constant-temperature wall (20°C). The latter case is realized in condensers and evaporators. Additionally, it is assumed that heat is transferred only through the corrugated plate, while the rest of the walls are considered adiabatic.

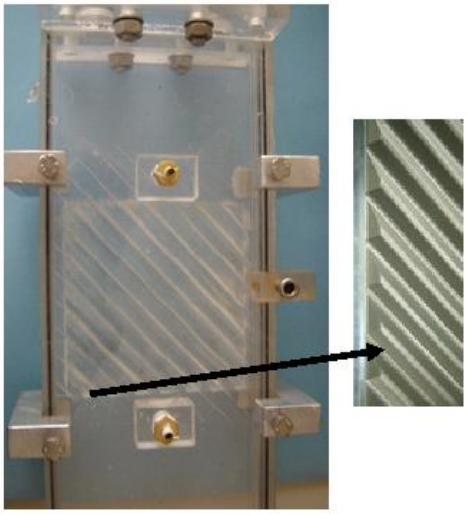

Figure 9 Simplified model and detail of the corrugated plate

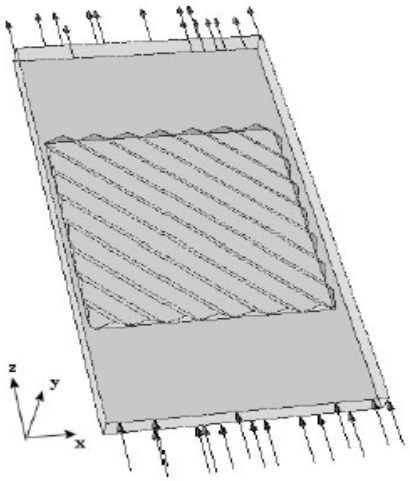

Figure 10 CFD model

A commercial CFD code, namely the *CFX ® 5.6* code developed by *AEA Technology*, was employed to explore its potential for computing detailed characteristics of this kind of flow. In general, the models used in CFD codes give reasonably good results for single-phase flow systems. The first step in obtaining a solution is the division of the physical domain into a solution mesh, in which the set of equations is discretised.

The grid size used is selected by performing a grid dependence study, since the accuracy of the solution greatly depends on the number and the size of the cells. The resulting mesh was also inspected for inappropriate generated cells (e.g. tetrahedral cells with sharp angles) and fixed, leading to a total number of 870,000 elements. The *SST* model was employed in the calculations for the reasons explained in the previous chapter. The mean velocity of the liquid phase was applied as boundary condition at the channel entrance (i.e. Dirichlet BC on the inlet velocity) and no slip conditions on the channel walls. A constant temperature boundary condition was applied only on the corrugated wall, whereas the rest of the walls are considered adiabatic. Calculations were performed on a *SGI O2* R10000 workstation with a 195MHz processor and 448Mb RAM. The *CFX ®5.6* code uses a finite volume method on a non-orthogonal body-fitted multi-block grid. In the present calculations, the *SIMPLEC* algorithm is used for pressure-velocity coupling and the *QUICK* scheme for discretisation of the momentum equations [31],[32].

Table 2 Simple Channel's plate geometric characteristics

Plate Length	0.200 m
Plate width	0.110 m
Maximum spacing between plates	0.010 m
Number of corrugations	14
Corrugation angle	45 ^{o}
Corrugation pitch	0.005 m
Corrugation width	0.014 m
Plate length before and after corrugations	0.050 m
Heat transfer area	2.7 x 10 $^{-2}$ m^2

The results of the present study suggest that fluid flow is mainly directed inside the furrows and follows them (***Figure 11a***). This type of flow behavior is also described by Focke & Knibbe[7], who made visual observations of the flow between two superposed corrugated plates ***(Figure 11b***). They confirm that the fluid, after entering a furrow, mostly follows it until it reaches the side wall, where it is reflected and enters the anti-symmetrical furrow of the plate above, a behavior similar to the one predicted by the CFD simulation. It seems that, in both cases, most of the flow passes through the furrows, where enhanced heat transfer characteristics are expected.

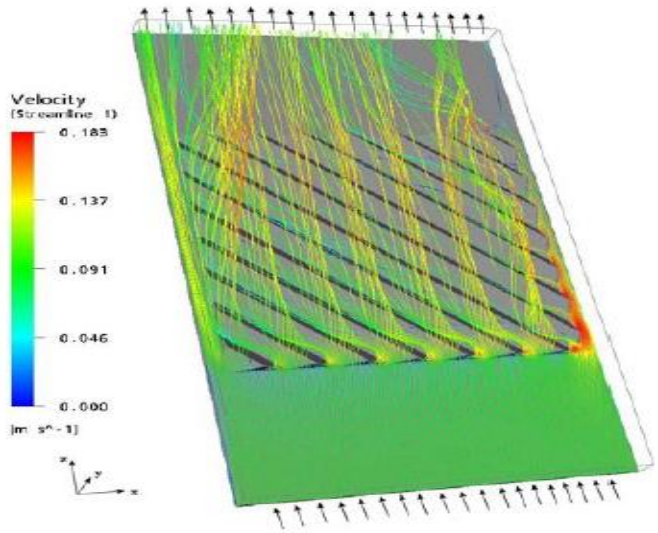

figure 11.a Typical flow pattern for the: a) simple channel, CFD results, Re=900

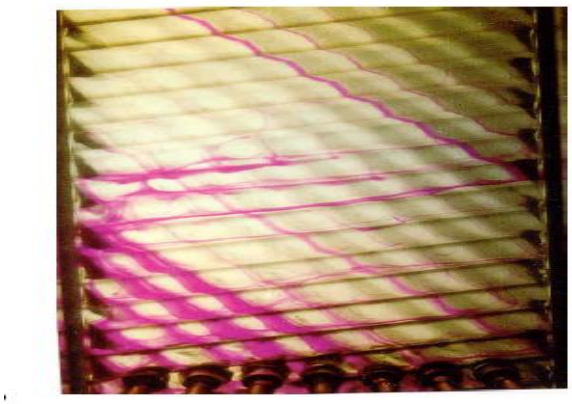

Figure 11.b) Flow visualization by Focke & Knibbe[7], Re=125

Figure 12 shows details of the flow inside a furrow for the simple model, where swirling flow is identified. This secondary flow is capable of bringing new fluid from the main stream close to the walls, augmenting heat transfer rates. Focke & Knibbe[18], who performed visualization experiments in similar geometries, also describe this kind of swirling flow. The values of the *z*-component of shear stress (***Figure13a***) increase with the Reynolds number –as expected–and the maximum value occurs at the crests of the corrugations. It may be argued that, during gas-liquid counter-current flow in such geometries, the shear stress distribution tends to prevent the liquid layer from falling over the crest of the corrugations and to keep it inside the furrows. The visual observations of Paras et al.[14] seem to confirm the above behavior. The heat flux through the wall of the corrugated plate was calculated by the CFD code. In addition, the local Nusselt number was calculated (by a user-Fortran subroutine) using the expression:

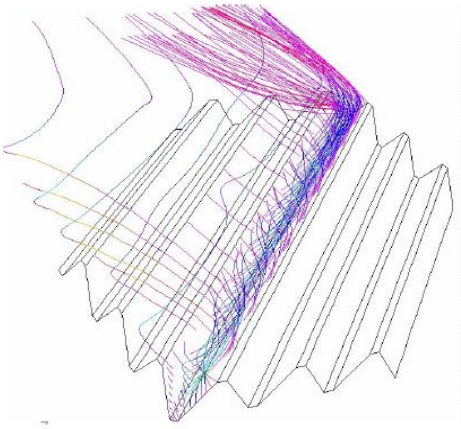

Figure 12 Swirling flow inside a furrow; Re=900

$$Nu_x = qd / (T_b - T_w)\, k \qquad (31)$$

Where *q'* is the local wall heat flux, *d* the distance between the plates at the entrance, *Tw* the wall temperature, *Tb* the local fluid temperature and *k* the thermal conductivity of the fluid. In addition to the local Nusselt number, mean Nusselt numbers were calculated as follows:

* A *mean Nu* calculated by numerical integration of the local *Nu* over the *corrugated* area ***only***, and
* An *overall* average *Nu* calculated using the total wall heat flux through the *whole* plate and the fluid temperatures at the channel entrance/exit.

The comparison of the values of the above Nusselt numbers shows that they do not differ more that 1%; therefore, the smooth part of the corrugated plate does not seem to influence the overall heat transfer. ***Figure 13b*** shows a typical local Nusselt number distribution over the corrugated wall for Re=900. All the Reynolds numbers studied exhibit similar distributions.

It is noticeable that local Nusselt numbers attain their maximum value at the top of the corrugations. This confirms the strong effect of the corrugations, not only on the flow distribution, but also on the heat transfer rate. To the best of author's knowledge, experimental values of heat transfer and pressure drop are very limited in the open literature for the corrugated plate geometry, since these data are proprietary. Therefore, the

data of Vlasogiannis et al.[16] were used to validate the simulation results. These data concern heat transfer coefficients measurements of both single (Re<1200) and two-phase flow in a plate heat exchanger with corrugated walls and a corrugation inclination angle of 60o. Heavner et al.[14] proposed a theoretical approach, supported by experimental data, to predict heat transfer coefficients of chevron-type plate heat exchangers. ***Figure14*** presents the experimental friction factors, obtained from the Plexiglas test section of ***Figure 9***, as well as the CFD predictions for the simple geometry studied, as a function of the Reynolds number. It appears that the experimental values follow a power law of the form:

$f = m\,Re^{-n}$ (32)

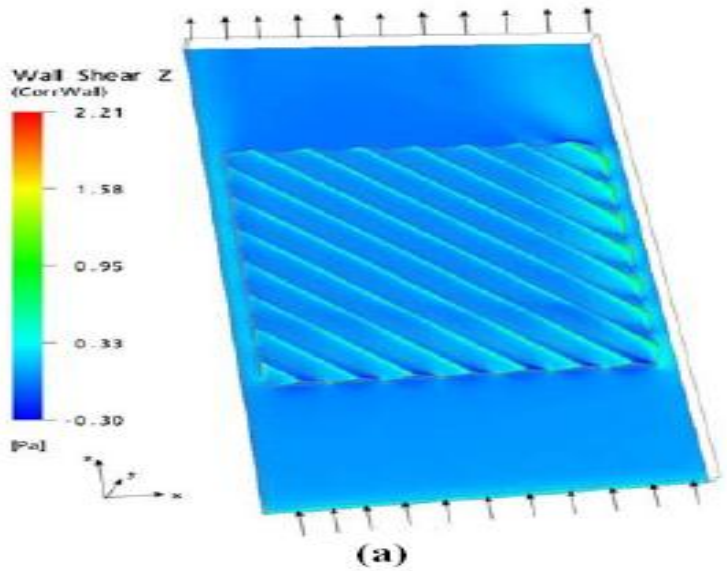

Figure 13. Typical results of the CFD simulation for Re=900; distributions of: (a) *z*-shear stress component

Where *m* and *n* constants with values 0.27 and 0.14 respectively. Heavner et al.[14] proposed a similar empirical correlation based on their experimental results on a single pass of a plate heat exchanger with 45o corrugation angle, but with two corrugated plates. In spite of the differences in geometry, it appears that the present results are in good agreement with the experimental data of Heavner et al.[14] (0.687 and 0.141 for the variables *m* and *n*, respectively).

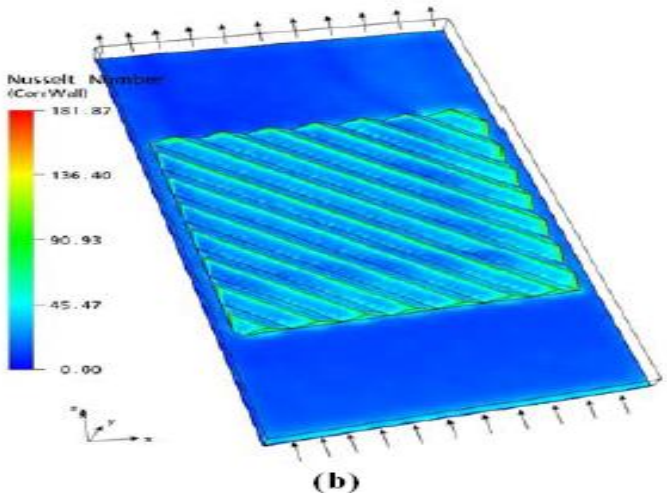

Figure 13. Typical results of the CFD simulation for Re=900; distributions of: (b) local Nusselt number

It must be noted that Focke et al.[15] , who also measured heat transfer coefficients in a corrugated plate heat exchanger having a partition of celluloid sheet between the two plates, reported that the overall heat transfer rate is the 65% of the corresponding value without the partition. ***Figure 15*** shows that the mean *j*-Colburn factor values calculated using the *overall* Nusselt number are practically equal to the 65% of the values measured by Vlasogiannis et al. This holds true for all Reynolds numbers except the smallest one (Re=400). In

the latter case the Nusselt number is greatly overpredicted by the CFD code. This is not unexpected, since the *two-equation turbulence* model is not capable to predict correctly the heat transfer characteristics for such low Reynolds number.The CFD results reveal that the corrugations enhance the heat transfer coefficient, whereas the pressure losses due to the augmentation of friction factor *f* are increased ***(Table 3)***, compared to a smooth-wall plate heat exchanger. Additionally, comparison of the normalized values of Nusselt number and the friction factor, with respect to the corresponding values for the smooth plate (*fsm*, *Nusm*), indicates that as the Reynolds number increases, heat transfer enhancement is slightly reduced, while the friction factor ratio, *f/f* , is increased. This is typical for plate heat exchangers with corrugations [16].

Table 3 Experimental values, calculated Nusselt numbers and normalised values of N_u and f

Re	Nu_{vlasog}	65% Nu_{vlasog}	Nu_{all}	Nu_{sm}	Nu_{ave}/ Nu_{sm}	F / f_{sm}
400	13.2	8.6	20.5	-	-	-
900	38.0	24.7	27.3	9.4	2.9	12.4
1000	41.2	26.8	28.6	10.2	2.8	12.8
1150	44.2	28.7	28.8	11.0	2.7	13.5
1250	46.8	30.4	30.9	11.7	2.7	13.9
1400	49.5	32.2	32.0	12.5	2.6	14.5

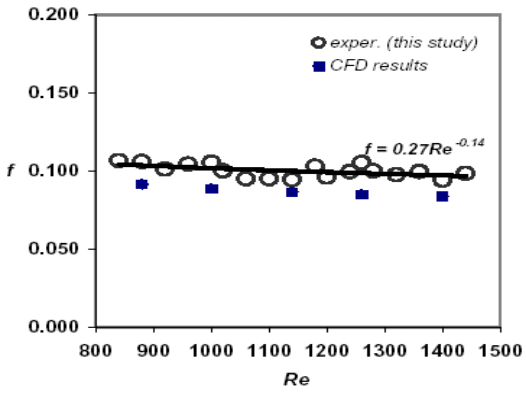

Figure 14. Comparison of friction factor predictions (CFD) with experimental data

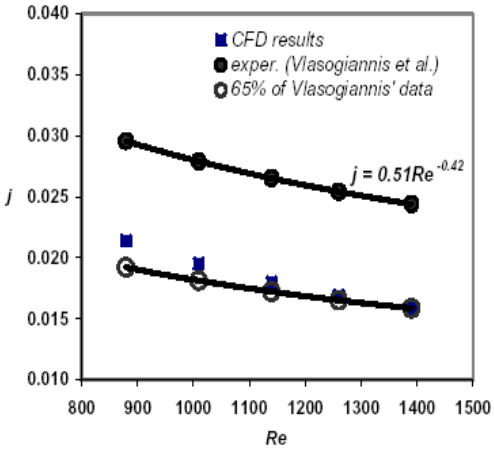

Figure 15. Comparison of *j*-Colburn factor predictions (CFD) with experimental data

VI. STUDY OF A HEAT EXCHANGER CHANNEL

The results for the simplified geometry confirm the validity of the CFD code and strongly encourage the simulation of a module (pass) consisting of two corrugated plates of a compact heat exchanger (***Figure16a***). In order to quantitatively evaluate the results of this simulation, the experimental setup of Vlasogiannis et al.[16]

was used as the design model (***Figure 16b***). Due to the increased computational demands, an AMD AthlonXP 1.7GHz workstation with 1GB RAM was used. The geometric characteristics of the new model are presented in ***Table 4.***

Table 4 Geometric characteristics of the model with two corrugated plates

Plate length	0.430 m
Plate width	0.100 m
Mean spacing between plates	0.024 m
Corrugation angles	60 ^{o}
Corrugation area length	0.352 m

Preliminary results of the present study, which is still in progress, are shown in ***Figure 17***. It is obvious that the herringbone design promotes a symmetric flow pattern (***Figure 16b***). Focusing on the left half of the channel (***Figure 17a***), a close-up of the flow streamlines (***Figure17b***) reveals a "*peacock-tail*" pattern as the liquid flows inside the furrows and over the corrugations. The same flow pattern, which is characteristic for this type of geometry, has also been observed by Paras et al.[14] in similar cross-corrugated geometries (***Figure17c***), where "dry areas" of ellipsoidal shape are formed around the points where the corrugations come into contact. The effect of fluid properties (e.g. surface tension, viscosity) on the shape and the extent of these areas, which are considered undesirable, will be examined in the course of this study.

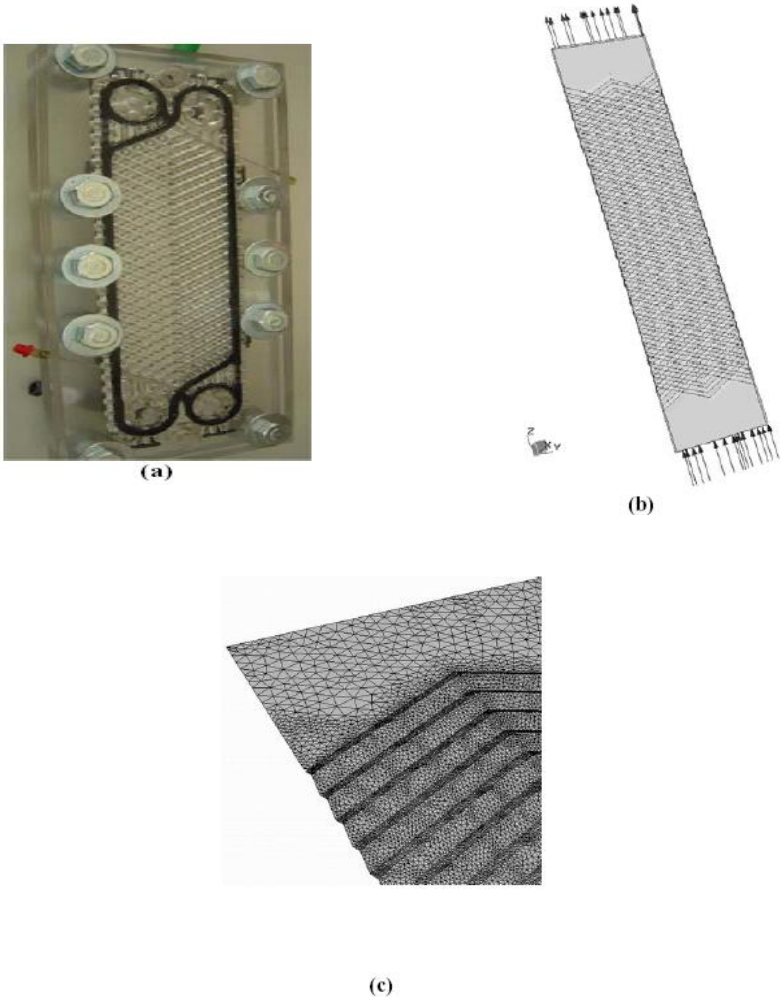

Figure 16. (a) Module of a corrugated plate exchanger; (b) The CFD model and (c) Detail of the grid distribution over the corrugated wall.

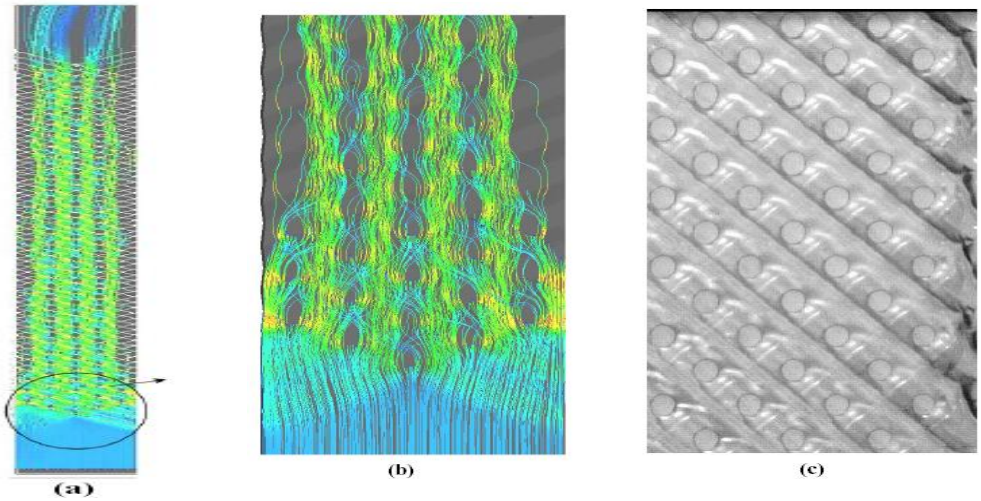

Figure 17. (a) Streamlines in the left half of the channel; (b) Close up of the flow pattern; (c) Photo of the flow in the cross-corrugated geometry [14]

VII. Conclusion

An experimental investigation has been conducted to measure the condensation heat transfer coefficient and the pressure drop of R410A and R22 in BPHEs with chevron angles of 20, 35, and 45 degrees. The experimental data were taken at two different condensation temperatures of 20°C and 30°C in the range of mass flux of 14-34 kg/m^{2}s with a heat flux of 4.7 -5.3 kW/m$^{2.}$

- Both the heat transfer coefficient and the pressure drop increased proportionally with the mass flux and the vapor quality and inversely with the condensation temperature and the chevron angle. Those effects must be carefully considered in the design of a BPHE due their opposing effects.
- A comparison of the data for R410A and R22 showed that the heat transfer coefficient for R410A was about 0 - 10 % larger and the pressure drop about 2- 21 % lower than those for R22. Therefore, R410A is a suitable alternative refrigerant for R22.

- Correlations for the Nusselt number and the friction factor with the geometric parameters were suggested for the tested BPHEs within 20 % (r.m.s. deviation: 10.9 %) for Nu and 15 % (r.m.s. deviation: 10 %) for f.

Although compact heat exchangers with corrugated plates offer many advantages compared to conventional heat exchangers, their main drawback is the absence of a general design method. The variation of their basic geometric details (i.e. aspect ratio, shape and angle of the corrugations) produces various design configurations, but this variety, although it increases the ability of compact heat exchangers to adapt to different applications, renders it very difficult to generate an adequate 'database' covering all possible configurations. Thus, CFD simulation is promising in this respect, as it allows computation for various geometries, and study of the effect of various design configurations on heat transfer and flow characteristics.

In an effort to investigate the complex flow and heat transfer inside this equipment, this work starts by simulating and studying a simplified channel and, after gaining adequate experience, it continues by the CFD simulation of a module of a compact heat exchanger consisting of two corrugated plates. The data acquired from former simulation is consistent with the single corrugated plate results and verifies the importance of corrugations on both flow distribution and heat transfer rate. To compensate for the limited experimental data concerning the flow and heat transfer characteristics, the results are validated by comparing the overall Nusselt numbers calculated for this simple channel to those of a commercial heat exchanger and are found to be in reasonably good agreement. In addition, the results of the simulation of a complete heat exchanger agree with the visual observations in similar geometries.

Since the simulation is computationally intensive, it is necessary to employ a cluster of parallel workstations, in order to use finer grid and more appropriate CFD flow models. The results of this study, apart from enhancing our physical understanding of the flow inside compact heat exchangers, can also contribute to the formulation of design equations that could be appended to commercial process simulators. Additional experimental work is needed to validate and support CFD results, and towards this direction there is work in progress on visualization and measurements of pressure drop, local velocity profiles and heat transfer coefficients in this type of equipment.

REFERENCES:

[1] X. Rong, M. Kawaji and J.G. Burgers, Two-phase header flow distribution in a stacked plate heat exchanger, *Proceedings ASME/JSME FED-Gas Liquid Flows* **225** (1995), pp. 115–122.

[2] H. Martin, 1996, A theoretical approach to predict the performance of chevron-type plate heat exchangers, Chemical Engineering and Processing: Process Intensification, Volume 35, Issue 4, Pages 301-310.

[3] G. J. Lee, J. Lee C. D. Jeon and O. K. Kwon. 1999. In: Plate Heat Exchanger with chevron angles ,Proceedings of the 1999 Summer Meeting of the SAREK, edited by C. S. Yim (SAREK, Nov.). p. 144.

[4] M. A. Kedzierski. 1997. Heat Exchanger Multiphase flow, Heat Transfer Engineering. Volume 5, issue 3 page 18: 25.

[5] Y. Y. Yan, H. C. Lio and T. F. Lin. 1999. Different Chevron angles in plate heat exchanger, of Heat and Mass Transfer. Volume 11, issue 4 pages 42: 93

[6] Y. Y. Hsieh and T. F. Lin. 2002.plate heat exchanger design theory, International journal of Heat and Mass Transfer. Volume 21, issue 9 pages 1033-45.

[7] Y. S. Kim. 1999. Plate heat exchanger design, M.S. Thesis. Yonsei University.

[8] S. Kakac and H. Liu. 1998. Heat Exchangers Selection, Rating and Thermal Design. CRC Press, Boca Raton. Volume 8, issue 9 pages 323-329

[9] R. J. Mo. 1982. Model of plate heat exchanger, ASME Journal of fluid engineering, Volume 11, issue 9 pages 173-179

[10] P. Vlasogiannis, G. Karajiannis. 2002. Compact heat exchangers, International journal Multiphase Flow.21, issue 9 pages 728: 757.

[11] T. J. Crawford, C. B. Weinberger and J. Weisman. 1985. heat exchangers International journal Multiphase Flow.21, issue 9 pages 291: 297.

[12] Shah, R.K., Wanniarachchi, A.S. (1991), Plate heat exchanger design theory, In: Buchlin, J.-M. (Ed.),Industrial Heat Exchangers, von Karman Institute Lecture Series 1991-04.

[13] Kays, W.M. & London, A.L. (1998), Compact heat exchangers, 3rd Ed. Krieger Publ. Co., Florida.

[14] Paras, S.V., Drosos, E.I.P., Karabelas, A.J, Chopard, F. (2001), "Counter-Current Gas/Liquid Flow Through Channels with Corrugated Walls–Visual Observations of Liquid Distribution and Flooding", World Conference on Experimental Heat Transfer, Fluid Mechanics & Thermodynamics, Thessaloniki, September 24-28.

[15] Ciofalo, M. Collins, M.W., Stasiek, J.A. (1998), Flow and heat transfer predictions in flow passages of air preheaters: assessment of alternative modeling approaches, In: Computer simulations in compact heat exchangers, Eds. B. Sunden, M.Faghri, Computational Mechanics Publ. U.K.

[16] Vlasogiannis, P., Karagiannis, G., Argyropoulos, P., Bontozoglou, V. (2002), "Air–water two-phase flow and heat transfer in a plate heat exchanger", Int. J. Multiphase Flow, 28, 5, pp. 757-772.

[17] Lioumbas, I.S., Mouza, A.A., Paras, S.V. (2002), "Local velocities inside the gas phase in counter current two-phase flow in a narrow vertical channel", Chemical Engineering Research & Design, 80, 6, pp. 667-673.

[18] Focke, W.W., Knibbe, P.G. (1986), "Flow visualization in parallel-plate ducts with corrugated walls", J.

[19] fluid Mech., 165, 73-77.

[20] Davidson, L. (2001), An Introduction to Turbulence Models, Department of Thermo and Fluid Dynamics, Chalmers University of Technology, Götemberg, Sweden.

[21] Menter, F., Esch, T. (2001), "Elements of Industrial Heat Transfer Predictions", 16th Brazilian Congress of Mechanical Engineering (COBEM), 26-30 Nov. 2001, Uberlandia, Brazil.

[22] AEA Technology (2003), CFX Release 5.6 User Guide, CFX International, Harwell, Didcot, UK.

[23] Wilcox,D(1988), "Reassessment of the scale-determining equation", AIAA Journal, 26,11.

[24] Mehrabian, M.A., Poulter, R. (2000), "Hydrodynamics and thermal characteristics of corrugated channels: computational approach", Applied Mathematical Modeling, 24**,** pp. 343-364.

APPENDIX

Nomenclature

A	heat transfer area of plate [m^2]
b	mean channel spacing [m]
C_p	constant pressure specific heat [J/kg K]
D	diameter [m]
f	friction factor
G	mass flux [kg/m^2s]

Ge	non-dimensional geometric parameter
g	gravitational acceleration [m/s^2]
h	heat transfer coefficient [W/m^{2}K]
i	enthalpy [J/kg]
j	superficial velocity [m/s]
L_c	distance between the end plates [m]
L_h	distance between the ports [m]
L_v	vertical length of the fluid path [m]
L_w	horizontal length of the plates [m]
LMTD	log mean temperature difference [°C]
m	mass flow rate [kg/s]
N_{cp}	number of channels for the refrigerant
N_{data}	total number of data
N_t	total number of plates
Nu	Nusselt number
Nu_{exp}	Nusselt number obtained from experiment
Nu_{pred}	Nusselt number obtained from correlation
p	plate pitch [m]
p_{co}	corrugation pitch [m]
Pr	Prandtl number [v]
Q	heat transfer rate [W]
q	heat flux [W/m^2]
Re	Reynolds number
T	temperature [°C]
t	plate thickness [m]
U	overall ht coefficient [W/m^2 K]
x	quality

Subscripts

a	acceleration
c	channel
Eq	equivalent
f	liquid
fg	difference the liquid phase and the vapor phase
fr	friction
g	vapor
in	inlet
lat	latent
m	mean
out	outlet
p	port
pre	pre-heater
r	refrigerant
s	static
sat	saturated
sens	sensible
w	water